# Physicochemical and Conformational Studies on BSA−Surfactant Interaction in Aqueous Medium

**ARTICLE** *in* LANGMUIR · APRIL 2009

Impact Factor: 4.46 · DOI: 10.1021/la803797x · Source: PubMed



**4 AUTHORS**, INCLUDING:

Indranil Chakraborty
St. Xavier's College, Kolkata
**25** PUBLICATIONS **915** CITATIONS
SEE PROFILE

Satya P Moulik
Jadavpur University
**298** PUBLICATIONS **7,378** CITATIONS
SEE PROFILE

Langmuir



Article

# Physicochemical and Conformational Studies on BSA#Surfactant Interaction in Aqueous Medium

Tanushree Chakraborty, Indranil Chakraborty, Satya P. Moulik, and Soumen Ghosh

*Langmuir*, **Article ASAP** • DOI: 10.1021/la803797x • Publication Date (Web): 03 February 2009



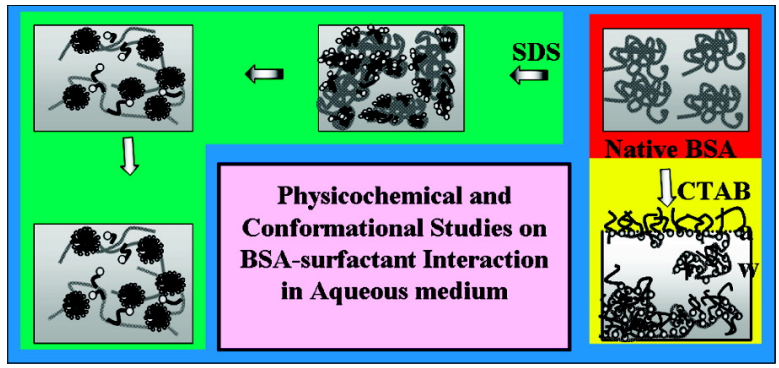


## More About This Article

Additional resources and features associated with this article are available within the HTML version:

- Supporting Information
- Access to high resolution figures
- Links to articles and content related to this article
- Copyright permission to reproduce figures and/or text from this article

View the Full Text HTML

# Physicochemical and Conformational Studies on BSA−Surfactant Interaction in Aqueous Medium

Tanushree Chakraborty, Indranil Chakraborty,† Satya P. Moulik, and Soumen Ghosh*

*Centre for Surface Science, Department of Chemistry, Jadavpur University, Kolkata-700 032, India*

*Received November 15, 2008. Revised Manuscript Received December 24, 2008*

In this paper, results of physicochemical studies on the interaction of bovine serum albumin (BSA) with alkyltrimethylammonium bromide (ATAB), pentaethylene glycol mono-*n*-dodecyl ether ($C_{12}E_5$), and sodium dodecyl sulfate (SDS) under the experimental conditions of phosphate buffer at pH 7 in the presence of 10 mM sodium bromide (NaBr), maintaining the ionic strength of the overall solution at $\mu = 0.015$ M, have been presented and discussed. Here, BSA−ATAB corresponds to a polyion−surfactant system bearing opposite charges. BSA precipitated out of the solution on addition of ATAB solution over a certain range of ATAB concentration, the concentration range being dependent on the particular member of the ATAB family. In our earlier reports on the precipitation of oppositely charged polymer−surfactant, the tensiometric profile for surfactant addition in polymer solution differed significantly from that expected from addition of surfactant in the dispersion medium. In the present study, the precipitation process could hardly affect the smoothness of the tensiometric profile. This indicates the interaction process is operative in bulk solution. Microcalorimetric profiles also evidenced an extra hump in the interaction profile at lower surfactant concentrations, without much affecting the dilution enthalpograms beyond micellization. This interaction appeared unimodal and the extent of interaction increased with increasing tail length of ATAB, evidencing the hydrophobic effect to be an important factor. Addition of salt (NaBr) also affected the nature of interaction: at lower concentration of NaBr, the interaction was mildly assisted, whereas 50 mM NaBr fairly assisted the interaction. The nonionic surfactant $C_{12}E_5$ modestly interacted with BSA. The anionic amphiphile SDS, on the other hand, interacted with BSA in two distinctly different stages, as evidenced from the tensiometric profile. The complexity of the BSA−SDS tensiometric isotherm compared to that of BSA−ATAB arose from the presence of cationic binding sites adjacent to hydrophobic patches of BSA in its native state, so that electrostatic and hydrophobic interactions can cooperatively operate side by side. The interfacial saturation occurred at a lower concentration in the presence of BSA compared to the normal cmc of SDS under identical solution conditions in the absence of BSA, which was slightly delayed for nonionic $C_{12}E_5$. The multitechnique approach evidenced that different experimental techniques probe different physicochemical phenomena and an attempt to show the concurrence of the break points in different techniques is only diluting the essence of this area.

## Introduction

Establishing a protein's structure in its native state is a complex proposition. Many physical methods are cumulatively necessary for its elucidation. Moreover, the structure of proteins varies significantly in solution and solid phases. Although many native protein structures are presently known at the level of atomic resolution, a clear understanding of the physical principles of their organization and stabilization in space is still lacking. A useful approach to this problem is studying the denaturation of the native structure by external probes. The commonly used denaturants are urea, guanidine hydrochloride, and ionic surfactants. The ionic surfactants bound to the oppositely charged sites (amino acid residue) denaturate native protein structure, leading to unfolding of the biopolymers at low denaturant concentrations. There is evidence that, at the initial stage, the interaction is of electrostatic nature, which causes the protein to unfold, resulting in the exposure of more binding sites. As surfactant concentration is increased, the binding becomes cooperative, and ultimately, the surfactants and their aggregates saturate the biopolymer.[1] Urea and guanidine hydrochloride affect the denaturing process in several ways,[2−6] one of which is affecting the water structure.[7] The process is therefore passive, and consequently, the required denaturant concentration is relatively large.

In mammals, albumin is synthesized by the liver and possesses a half-life in circulation of 19 days.[8,9] Its primary structure consists of 580 amino acids[10] and the secondary structure consists of 67% α-helix with six turns and 17 disulfide bridges.[11] The proposed structure of bovine serum albumin (BSA) is heart shaped,[12] consisting of three homologous domains (I, II, III), which are divided into nine loops (L1−L9) by the disulfide bonds. The loops in each domain are made up of a sequence of large−small−large loops forming a triplet. Each domain is composed of two subdomains. The subdomains share a number of common features, viz., a hydrophobic face, a cluster of basic amino acid residues, and protein residues at tops of the long loops. It is also established that each subdomain is unique and exhibits a certain degree of binding specificity.[10,13,14] The isoelectric pH of BSA is 5.4.[14] Serum albumin is the most

* To whom correspondence should be addressed. E-mail: gsoumen70@hotmail.com.

† Department of Chemistry, St. Xavier's College, Kolkata-700 016, India.

(1) Jones, M. N. *Chem. Soc. Rev.* **1992**, *21*, 127.
(2) Timasheff, S. N. *Annu. Rev. Biphys. Biomol. Struct.* **1993**, *22*, 67.
(3) Ramos, C. H. I.; Baldwin, R. L. *Protein Sci.* **2002**, *11*, 1771.
(4) Bostrom, M.; Williams, D. R. M.; Ninham, B. W. *Biophys. J.* **2003**, *85*, 686.
(5) Russo, A. T.; Rosgen., J.; Bolen, D. W. *J. Mol. Biol.* **2003**, *330*, 851.
(6) Schellman, J. A. *Biophys. J.* **2003**, *85*, 108.
(7) Das Gupta, P. K.; Moulik, S. P. *J. Phys. Chem.* **1987**, *91*, 5826.
(8) Carter, D. C.; Chang, B.; Ho, J. X.; Keeling, K.; Krishnasami, Z. *Eur. J. Biochem.* **1994**, *226*, 1049.
(9) Min He, X.; Carter, D. C. *Nature* **1992**, *358*, 209.
(10) Brown, J. R.; Shockley, P. In *Lipid−Protein Interactions*; Jost, P., Griffith, O. H., Eds.; Wiley: New York, 1982; Vol. 1.
(11) Narazaki, R.; Otagiri, M. *Biochim. Biophys. Acta* **1997**, *1338*, 275.
(12) Bos, O. J. M.; Labro, J. F. A.; Fischer, M. J. E.; Witling, J.; Janssen, L. H. M. *J. Biol. Chem.* **1989**, *264*, 953.

10.1021/la803797x CCC: $40.75 

abundant protein in plasma contributing about 80% to the colloid osmotic blood pressure.[15] It also maintain the blood pH.[15] BSA and human serum albumin (HSA) display approximately 76% sequential homology and a strictly conserved repeating pattern of disulfides.[14] On the basis of the dominant presence of amino acids with some specific nature in each domain, they have a preference toward binding for some specific ligands according to Curry et al.,[16] who studied the crystal structure of HSA in the combined state with several fatty acids and biological substances, etc.

Fatty acid transportation appears to be the most important function of BSA. Fatty acids preferentially interact with domain I, containing seven high-energy sites[17,18] for accommodating long chain fatty acid ligands. A number of binding studies have focused on the multifunctional binding properties of BSA[10,12,19−21] with a wide variety of molecules. The binding function assists in transporting soluble substances between tissues and organs, playing an important role in the deposition of a variety of endogenous and exogenous substances in blood[22] due to the existence of binding regions of different specificities.[23]

BSA−SDS interaction has been extensively studied by fluorescence spectrophotometry.[24−29] Cistola et al.[30] studied BSA−fatty acids interaction using an NMR technique. The NMR study by Turro et al.[24] advocated the necklace-bead model (at pH 5.4) with the biopolymer affecting the mobility of lower surfactant aggregates. SAXS[31] and SANS[32] study of BSA−SDS complex indicated retention of native BSA structure at low SDS concentration below the critical aggregation concentration (cac); beyond 5 mM SDS, BSA structure changes, and small micelle-like aggregates are formed at [SDS] > 10 mM. Shinagawa et al.[33] showed that BSA−SDS complex structure at pH 7.1 is consistent with both the necklace model[34] and the protein-decorated micelle structure model.[35] In the later model, the polypeptide is assumed to decorate the SDS cluster rather than penetrating it, as in the necklace model. Gelamo et al.[36] have used the SAXS technique to show efficient unfolding of BSA by cetyltrimethylammonium chloride (CTAC) compared to SDS at pH 7. The calorimetric (ITC and DSC) study of the interaction between BSA and SDS or dodecyltrimethylammonium bromide (DTAB) by Kelley and McClements[37] revealed stabilization of native BSA structre upon monomeric adsorption of SDS at low [SDS] at pH 7 and its unfolding at higher [SDS], whereas DTAB caused unfolding of the protein structure from the very beginning. Binding isotherms of BSA with several surfactants are already reported in the literature.[1,38,39]

We have systematically studied the protein−surfactant interaction (including their physicochemical and conformational changes).[40−46] In this paper, we report a detailed tensiometric, circular dichroic, turbidimetric, viscometric, and microcalorimetric study on the interaction of BSA with cationic, nonionic, and anionic surfactants with same tail length ($C_{12}$). The effect of variation in tail length within the ATAB family employing dodecyl, tetradecyl, and hexadecyl, or cetyltrimethylammonium bromide has also been examined. Additionally, the effect of added NaBr on the interaction between BSA and DTAB has been investigated. Microcalorimetry is insensitive to where the process is occurring but registers every enthalpic response. The interfacial probing is by tensiometry and the probing in bulk solution is by viscometry and turbidimetry. All these methods showed different features of the interaction process due to phenomenological differences in interaction in bulk and at the interfacial solution. Microcalorimetry also produced immense information on the BSA−surfactant interaction process.

## Experimental Section

**Materials.** BSA (MW = 66 000, purity >98.5%), hexadecyltrimethylammonium bromide (purity >98%) (CTAB), and tetradecyltrimethylammonium bromide (purity >96.5%) (TTAB) were purchased from Sigma. Dodecyltrimethylammonium bromide (DTAB) (96% pure) was a product of Alfa Aesar, and sodium dodecyl sulfate (98% pure) was purchased from Fluka, Switzerland. The nonionic pentaethylene glycol mono-*n*-dodecyl ether ($C_{12}E_5$) was a product of Nikkol, Japan. Disodium hydrogen phosphate ($Na_2HPO_4$), sodium dihydrogen phosphate ($NaH_2PO_4$), and sodium bromide (NaBr) were AR grade products of SRL. All chemicals were used as received. All solutions were prepared in phosphate buffer solution of pH 7 in presence of 10 mM NaBr prepared with doubly distilled water, maintaining the ionic strength of the overall solution at $\mu = 0.015$ M (hereafter referred to as the phosphate buffer solution) unless otherwise mentioned. Protein concentrations in "grams of BSA per 100 mL of solution" are reported as "% (w/v)".

**Methods.** *Tensiometry.* Tensiometric measurements were taken in a calibrated du Noüy Tensiometer (Krüss, Germany) by the ring detachment technique. Ten milliliters of 0.025% (w/v) BSA solution in phosphate buffer was taken in a thermostated (303 ± 0.1 K) container and the desired concentration of buffered ($\mu = 0.015$ M) surfactant solution was stepwise added as required. Measurements were taken manually, allowing a 30 min time interval for equilibration.

(13) Min He, X.; Carter, D. C. *Nature* **1992**, *358*, 209.
(14) Peters, T. In *Advances in Protein Chemistry*; Academic Press: New York, 1985; Vol. 37, pp 161.
(15) Anfinsen, C. B.; Edsall, J. T.; Richards, F. M. In *Advances in Protein Chemistry*; Academic Press: New York, 1985; Vol. 37.
(16) Curry, S.; Mandelkow, H.; Brich, P.; Franks, N. *Nat. Struct. Biol.* **1998**, *5*, 827.
(17) Fasano, M.; Curry, S.; Terreno, E.; Galliano, M.; Fanali, G.; Narciso, P.; Notari, S.; Ascenzi, P. *IUMAB Life* **2005**, *57*, 787.
(18) Simard, J. R.; Zunszain, P. A.; Ha, C.-E.; Yang, J. S.; Bhagavan, N. V.; Petitpas, I.; Curry, S.; Hamilton, J. A. *Proc. Nat. Am. Sci. USA* **2005**, *102*, 17958.
(19) Kragh-Hansen, *Pharmacol. Rev.* **1981**, *33*, 17.
(20) Foster, J. F. In *Albumin Structure, Function and Uses*; Roesnoer, V. M., Oratz, M., Rothschild, M. A., Eds.; Pergamon: Oxford, 1977; pp 53.
(21) Valstar, A.; Almgren, M.; Brown, W.; Vasilescu, M. *Langmuir* **2000**, *16*, 922.
(22) Kosa, T.; Maruyama, T.; Otagiri, M. *Biochim. Biophys. Acta* **1997**, *1338*, 275.
(23) Moreno, F.; Cortijo, M.; Jimenez, J. G. *Photochem. Photobiol.* **1999**, *69*, 8.
(24) Turro, N. J.; Lei, X.-G.; Ananthapadmanabhan, K. P.; Aronson, M. *Langmuir* **1995**, *11*, 2525.
(25) Vasilescu, M.; Angelescu, D.; Almgren, M.; Valstar, A. *Langmuir* **1999**, *15*, 2635.
(26) Shweitzer, B.; Zanetti, D.; Itri, R. *J. Colloid Interface Sci.* **2004**, *277*, 285.
(27) Xu, Q.; Keiderling, T. A. *Protein Sci.* **2004**, *13*, 2949.
(28) Honda, C.; Kamizano, H.; Matsumoto, K.; Endo, K. *J. Colloid Interface Sci.* **2004**, *278*, 310.
(29) Chakraborty, A.; Seth, D.; Setuna, P.; Sarkar, N. *J. Phys. Chem. B.* **2006**, *110*, 16607.
(30) Cistola, D. P.; Small, D. M.; Hamilton, J. A. *J. Biol. Chem.* **1987**, *262*, 10980.
(31) Santos, S. F.; Zanetti, D.; Fischer, H.; Itri, R. *J. Colloid Interface Sci.* **2003**, *262*, 400.
(32) Chen, S. H.; Teixeiria, J. *Phys. Rev. Lett.* **1986**, *57*, 2583.
(33) Shinagawa, S.; Sato, M.; Kameyama, K.; Takagi, T. *Langmuir* **1994**, *10*, 1690.
(34) Shirahama, K.; Tsujii, K.; Takagi, T. *J. Biochem.* **1974**, *75*, 309.
(35) Ibel, K.; May, R. P.; Kirschner, K.; Sxadkowski, H.; Mascher, E.; Lundhahl, P. *Eur. J. Biochem.* **1990**, *190*, 311.
(36) Gelamo, E. L.; Itri, R.; Alonso, A.; da Silva, J. V.; Tabak, M. *J. Colloid Interface Sci.* **2004**, *277*, 471.
(37) Kelley, D.; McClements, D. J. *Food Hydrocolloids* **2003**, *17*, 73.
(38) Gelamo, E. L.; Tabak, M. *Spectrochim Acta Part A.* **2000**, *56*, 2255.
(39) Moosavi-Movahedi, A. A.; Bordbar, A. K.; Taleshi, A. A.; Naderimanesh, H. M.; Ghadam, P. *Int. J. Biochem. Cell Biol.* **1996**, *28*, 991.
(40) Chatterjee, A.; Moulik, S. P.; Majhi, P. R.; Sanyal, S. K. *Biophys. Chem.* **2002**, *98*, 313.
(41) Ghosh, S.; Banerjee, A. *Biomacromolecules* **2002**, *3*, 9.
(42) Ghosh, S. *J. Surf. Sci. Technol.* **2003**, *19*, 167.
(43) Ghosh, S. *Colloid Surf. A* **2005**, *264*, 6.
(44) Ghosh, S. *Colloid Surf. B* **2005**, *41*, 209.
(45) Ghosh, S. *Colloid Surf. B* **2008**, *66*, 178.
(46) Chakraborty, T.; Chakraborty, I.; Moulik, S. P.; Ghosh, S. *J. Phys. Chem. B* **2007**, *111*, 2736.

No more than 1.0 mL of surfactant solution was added to BSA solution. The detailed procedure of measurement of surface tension has been reported earlier.[46−50] Duplicate experiments were performed for each run, and close resemblance between the two was observed. The $\gamma$ values were accurate within $\pm 0.1$ mN m$^{-1}$. The $\gamma$ values are experimental data without any correction, as the absolute $\gamma$ value for BSA solution under similar experimental conditions is beyond our knowledge.

*Circular Dichroism.* Far- and near-UV circular dichroism (CD) experiments were performed in a Jasco, J-815 CD spectropolarimeter attached to a chiller to control the temperature of the electronic circuit (sample temperature 303 K). The instrument was calibrated with an aqueous solution of *d*-10-camphorsulfonic acid using a slit width of 1 nm and a scan speed of 50 nm min$^{-1}$. A 0.2 mL aliquot of 0.025% (w/v) BSA at pH 7 was taken in a cuvette of 1 mm path length for measuring the far- and near-UV CD spectra in the range between 200 and 320 nm, and consequently, concentrated surfactant solutions were added to study the conformational changes in the secondary and tertiary structures of BSA at the different stages of interactions, respectively. The reported spectra were the average of five scans.

*UV−Vis Spectrophotometry.* A UV−visible (1601) Shimadzu spectrophotometer operating in dual-beam mode was employed for spectral measurements using a matched pair of quartz cuvettes of path length 1 cm under thermostated condition (303 ± 0.1 K). For the turbidimetric experiments, the instrument was baseline corrected using buffered BSA solution in either cuvette, and the experiments were performed using buffered BSA solution as the control, so that the variation in absorbance due to addition of surfactant solution in BSA solution is due to formation of polymer−surfactant. Surfactant solution was progressively added to the sample cell [consisting of 3 mL of 0.025% (w/v) BSA solution] as required. Optical density at each stage of surfactant addition was measured at $\lambda_{max} = 450$ nm. The dilution effect of the biopolymer solution hardly affected the nature of turbidimetric profile.

*Viscometry.* The viscometric experiments were performed using a Cannon−Fenske capillary viscometer with a flow time of 118 s for 10 mL of water under thermostated condition at 303 ± 0.1 K. Ten milliliters of 0.025% (w/v) BSA solution was taken in the viscometer, and concentrated surfactant solution was progressively added into it in stages with a Hamilton microsyringe, mixed thoroughly, allowing for equilibration, and the flow times were noted. The average of three consecutive measurements was considered for each run. The results were associated with a standard deviation of ±5%. Viscosity of the solution relative to that of the buffered BSA solution was considered as the ratio of flow time of the respective solutions at different stages of surfactant addition.

*Microcalorimetry.* An OMEGA, ITC, microcalorimeter (MicroCal, Northampton, MA) was used for thermometric measurements. A concentrated solution (~20 times its cmc in aqueous medium) of the surfactant was taken in the microsyringe and was added after equal time intervals of 210 s in multiple steps (32 additions) to 1.325 mL of 0.025% (w/v) BSA solution of pH 7 taken in the calorimeter cell under constant stirring (300 rpm) condition. Identical BSA solution (1.6 mL, corresponding to the final volume of the reaction cell) was taken in the reference cell. During titration with surfactant solution, the heat change in the sample cell disturbs the thermal equilibrium between the reference cell and the sample cell, and the instrument adjusts the thermal equilibrium of the two cells. The power required to achieve this thermal equilibrium is digitalized as the enthalpy change per mole of the surfactant per injection using the ITC software. The experiment for surfactant dilution was also performed with the same injection matrix as that of the interaction experiment, taking buffer solution in the reference cell. Each run was duplicated to check reproducibility. The temperature of the Neslab RTE100 circulating water bath was maintained at 303 ± 0.1 K; the temperature in the cell compartment in the calorimeter was automatically adjusted to an accuracy of ±0.01 K. The enthalpy of interaction (for BSA−SDS system) was obtained by subtracting the heat of surfactant dilution in buffer solution from the heat associated with surfactant dilution in BSA solution.

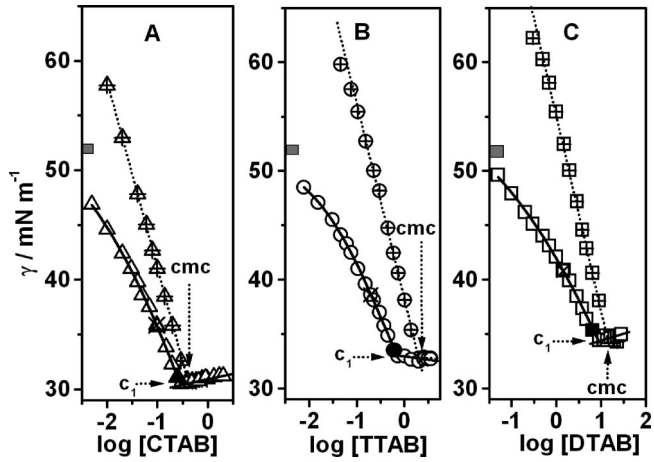


**Figure 1.** Tensiometric profiles for 0.025% (w/v) BSA−ATAB (A, CTAB; B, TTAB; C, DTAB) interaction in 10 mM phosphate buffer of pH 7 at 303 K. The crossed symbols/dotted lines and open symbols/solid lines represent pure and interaction profiles respectively with break points cmc and $c_1$. The surface tension value for 0.025% (w/v) is represented as a gray square in each profile on the $\gamma$ axis. In the interaction profile, the appearance of turbidity (x-ed symbol) and the disappearance of turbidity (solid symbol) are also indicated.

## Results and Discussion

The present study on BSA [0.025% (w/v)]−amphiphile interactions was carried out at pH 7 (phosphate buffer) in the presence of 10 mM NaBr (so that total ionic strength of the overall solution becomes 0.015 M), unless otherwise mentioned. Because the pH of BSA was above its isoelectric point,[14] the overall charge on the protein was negative. At neutral pH, BSA has a overall −18 surface charge[52] arising out of a balance of a large number of positive and negative charges over the protein surface. The BSA−ATAB, therefore, represents an oppositely charged polymer−surfactant system where both electrostatic and hydrophobic interactions between the components was expected. For the nonionic ($C_{12}E_5$) and anionic (SDS) surfactants, mainly the hydrophobic interaction was expected to be operative.

**BSA−ATAB Interaction.** Formation of surfactant-saturated monolayer at the air/solution interface is a valid approximation as the critical micellar concentration (cmc) tensiometrically when the interfacial saturation and bulk micellization processes are coherent. The surfactant concentration at the breakpoint in the surface tension ($\gamma$) vs natural logarithm of surfactant concentration (log[surfactant]) profile corresponded to the cmc. Tensiometric profiles for addition of ATABs to buffer solution under identical experimental conditions are illustrated with crossed symbols and dotted lines in Figure 1, and the cmc values were found to decrease with increasing surfactant chain length (Table 1), evidencing that the self-aggregation process is hydrophobicity-driven. The hydrophobic tails of monomeric surfactants are encapsulated in icebergs of structured water molecules, called the hydrophobic hydration. During self-association, this structured layer of hydrophobic solvation is disrupted, leading to an increase in entropy of the overall system, which drives the micellization process.[52] The ionic strength of the buffer solution lowered the

(47) Moulik, S. P.; Ghosh, S. *J. Mol. Liq.* **1997**, *72*, 145.
(48) Ghosh, S.; Moulik, S. P. *J. Colloid Interface Sci.* **1998**, *208*, 357.
(49) Chakraborty, T.; Chakraborty, I.; Ghosh, S. *Langmuir* **2006**, *22*, 9905.
(50) Ghosh, S.; Chakraborty, T. *J. Phys. Chem. B* **2007**, *111*, 8080.
(51) Chakraborty, T.; Ghosh, S.; Moulik, S. P. *J. Phys. Chem. B* **2005**, *109*, 14813.
(52) Ted Lee C. Jr.; Smith, K. A.; Hatton, T. A. *Biochemistry* **2005**, *44*, 524.

**Table 1. Critical Micellar Concentration (cmc) and Other Physicochemical Parameters of Pure and Interaction of ATABs with 0.025% BSA at pH 7 Using Different Techniques at 303 K**

| methods | | | CTAB | TTAB | DTAB |
|---|---|---|---|---|---|
| surface tension | pure | cmc/mM | 0.40 | 2.01 | 13.2 |
| | | $\gamma_{cmc}$/mN m$^{-1}$ | 30.9 | 32.6 | 34.8 |
| | | $\Gamma_{max}^{cmc} \times 10^6$/ mol m$^{-2}$ | 2.98 | 3.14 | 1.64 |
| | | $A_{min}^{cmc}$/nm$^2$ molecule$^{-1}$ | 0.56 | 0.53 | 1.01 |
| | interaction | $c_1$/mM | 0.28 | 0.74 | 6.26 |
| | | $\gamma_{c_1}$/mM | 30.5 | 32.9 | 33.8 |
| | | $\Gamma_{max}^{c_1} \times 10^7$/ mol m$^{-2}$ | 20.4 | 18.9 | 9.02 |
| | | $A_{min}^{c_1}$/nm$^2$ molecule$^{-1}$ | 0.81 | 0.88 | 1.84 |
| cd | pure | α-helix content/% | | 67 | |
| | interaction | α-helix content/% | | | |
| | | before $c_0$ | 46 | 46 | 49 |
| | | beyond $c_1$ | 12 | 16 | 15 |
| viscosity | pure | $c_{min}$/mM | 0.16 | 0.50 | 5.65 |
| | interaction | $c_{sat}$/mM | 0.42 | 1.00 | 3.63 |
| turbidimetry | interaction | $c_0$/mM | 0.09 | 0.22 | 1.85 |
| | | $c_T$/mM | 0.15 | 0.47 | 4.17 |
| | | $c_R$/mM | 0.27 | 0.81 | 7.98 |
| | | $A_{c_T}$ | 0.11 | 0..07 | 0.06 |
| microcalorimetry | pure | cmc/mM | 0.42 | 2.39 | 11.9 |
| | | $\Delta H_m$/ kcal mol$^{-1}$ | −2.9 | −1.3 | −0.7 |
| | interaction | $c_{sat}$/mM | 0.46 | 1.05 | 3.44 |
| | | $\Delta H_{c_{sat}}$/ kcal mol$^{-1}$ | −1.8 | −0.9 | −0.1 |
| | | cmc′/mM | 0.68 | 2.70 | 10.43 |
| | | $\Delta H_{cmc'}$/ kcal mol$^{-1}$ | −2.3 | −0.8 | −0.8 |

cmc of pure ATABs compared to that in pure water[53] by way of neutralizing the headgroup charge of the monomers and hence stabilizing the aggregates either in bulk (micelles) or at interface (monolayer).

The slope of the tensiometric profile near the cmc is a measure of interfacial adsorption efficacy of the surfactant, is quantified by the Gibbs surface excess ($\Gamma_{max}^{cmc}$), and is given by

$$\Gamma_{max}^{cmc} = -\left(\frac{1}{2.303nRT}\right)\lim_{C\to cmc}\left(\frac{\delta\gamma}{\delta \log C}\right) \quad (1)$$

where $C$ is the total amphiphile concentration in solution and $n = 1$ in all the cases,[55,56] $R$ is the universal gas constant, and $T$ is the absolute temperature. Here, we have neglected the contribution of counterions and the inorganic ions (from NaBr and buffer), as they have no preference toward interfacial adsorption. A crude approximation may be the degree of counterion condensation ($g$) at micellar surface obtained from conductometry, which seems vague as the radius of curvature of micellar surface differs significantly from that of the air/solution interface and this curvature considerably affect the adsorption behavior.[55] The minimum area of exclusion per surfactant monomer at the saturated air/solution interface ($A_{min}$) was calculated from the equation

$$A_{min} = 10^{18}/(\Gamma_{max}^{cmc} N_0) \quad (2)$$

where $N_0$ is Avogadro's number and the factor $10^{18}$ arises as a conversion factor of area from m$^2$ to nm$^2$. Among the ATABs, the efficacy toward interfacial adsorption, as quantified by $\Gamma_{max}^{cmc}$, remained more or less similar. This is again reflected in a similarity in compactness of air/solution interfacially adsorbed film as observed in $A_{min}^{cmc}$ (Table 1). The interfacial tension of BSA solution under study was ∼52 mN m$^{-1}$, showing feeble surface activity of BSA in solution.

Tensiometric profiles for BSA−ATAB interaction look fairly simple (Figure 1, solid line, open symbol) compared to our previous studies with oppositely charged polymer−surfactant systems.[46,49] The present tensiometric isotherm for ATAB addition in buffered BSA solution consists of a single break at a lower ATAB concentration compared to the cmc of pure ATABs in buffer solution. We denote the ATAB concentration corresponding to the saturation in $\gamma$ value as $c_1$. The interface in this regime is mostly populated by monomeric surfactant supported on polymer chain (Scheme 1).

Turbidity (coacervation) appeared during the course of BSA−ATAB interaction as a result of charge neutralization onto the biopolymer through electrostatic interaction with surfactant headgroup and consequent depletion of water of solvation. The ATAB concentration corresponding to the appearance of visual turbidity and its disappearance are marked in the tensiometric profiles with enlarged x-ed (×) and solid symbols, respectively. The ATAB concentration corresponding to the saturation of interfacial tension ($\gamma$) appeared very close (slightly greater) to the turbidity disappearance points of the solution, similar to that reported in our earlier study.[49] Gibbs surface excess at $c_1$ ($\Gamma_{max}^{c_1}$) was calculated from the slope of the linear portion of the $\gamma$ vs log[ATAB] profile, as also reported earlier in poly-L-lysin−SDS,[57] pepsin−CTAB,[46] sodium carboxymethylcellulose (NaCMC)−CTAB,[49] and gelatin−ATAB[58] systems. The area of exclusion per surfactant monomer at $c_1$ ($A_{min}^{c_1}$) was similarly calculated using eq 2. The interfacial parameters are included in Table 1.

The feeble surface activity of BSA under studied condition is revealed by a lower surface tension (∼52 mN m$^{-1}$, represented by a gray square symbol in all the tensiometric profiles) compared to the buffer solution (∼64 mN m$^{-1}$). The tensiometric profiles indicated that BSA fairly affected $\gamma$ of water by way of interfacial adsorption. The ATABs decreased it further also by way of adsorption onto the oppositely charged amino acid sites on BSA. The less steep slope with a convex appearance [compared to linear decrease for dilution of ATABs in buffer, as indicated by crossed (+) symbols and dotted lines in Figure 1] at the initial part of the interaction process and a lowering of $\gamma$ of the solution at a low ATAB concentration relative to that of pure ATAB in buffered solution (open symbols/solid line and crossed symbols/broken line in Figure 1) implied partial expulsion of the protein from the interface. Ultimately, the surface tension reached a minimum. The presence of BSA at the interface helped to reduce $\gamma$, and consequently, the ATAB concentration required to saturate the interface ($c_1$) was lower compared to the cmc in buffer. Similar behavior was observed by Tomasic et al.[54] in surfactant−synthetic polymer system and by us in pepsin−CTAB system.[46] The decreased $c_1$ compared to cmc, difference in $\Gamma_{max}^{cmc}$, $\Gamma_{max}^{c_1}$ and $A_{min}^{cmc}$, $A_{min}^{c_1}$ resulted from the polyelectrolyte-like behavior of BSA with adsorbed oppositely charged $ATA^+$ ions which, in turn, facilitated the charge neutralization and increased hydrophobicity of the BSA−ATAB complex, making $c_1$ < cmc. $\gamma_{cmc} \sim \gamma_{c_1}$ reflected that the presence of BSA could not significantly alter the topology of the surfactant-saturated monolayer, whereas $c_1$ < cmc reflected

(53) Menger, F. M. *Acc. Chem. Res.* **1979**, *12*, 111.
(54) Tomasic, V.; Tomasic, A.; Smii, I.; Filipovic-Vincent, N. *J. Colloid Interface Sci.* **2005**, *285*, 342.
(55) Das, C.; Chakraborty, T.; Ghosh, S.; Das, B. *Colloid Polym. Sci.* **2008**, *286*, 1143.
(56) Chattoraj, D. K.; Pal, R. P. *Indian J. Chem.* **1972**, *10*, 410.
(57) Buckingham, J. H.; Lucassen, J.; Hollway, F. *J. Colloid Interface Sci.* **1978**, *67*, 423.
(58) Mitra, D.; Bhattacharyya, S. C.; Moulik, S. P. *J. Phys. Chem. B.* **2008**, *112*, 6609.

**Scheme 1. Schematic Representation of BSA−ATAB Interaction[a]**

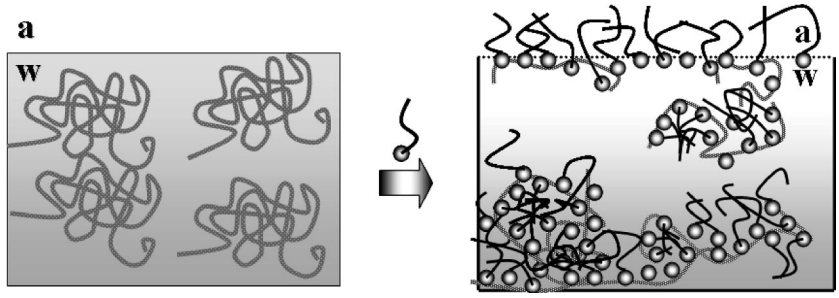


[a] ATAB is very efficient in unfolding BSA under the experimental conditions, leading to a unimodal coacervation process.

**Scheme 2. Presence of Polymer−Surfactant Complex at the Air/Solution Interface Decreases the Number Density of Surfactant Monomer at the Interface, Leading to a Decrease in Compactness of the Monolayer**

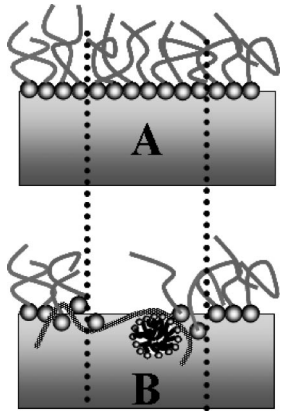


preferred interfacial adsorption tendency of the surfactant in the presence of the polymer−surfactant complex.[59−61] Moreover, since $c_1$ is greater than the ATAB concentration corresponding to the resolubilization process, participation of a fraction of BSA−ATAB complex at interfacial saturation can also be expected. The appearance of turbidity did not affect the smoothness of the tensiometric isotherm, suggesting that the coacervation process predominantly take place in bulk solution (Scheme 1). As per our earlier works on NaCMC−CTAB[49] and pepsin−CTAB,[46] the surfactants initially adsorbed onto the peripheral high-affinity binding sites of the folded polymers and hence increased the hydrophobicity of the polymer−surfactant complex, making them prone to interfacial adsorption. A further mode of binding involving the unfolded polymer is essential for coacervation. For BSA−ATAB interaction, ATABs induce unfolding of native BSA structure by its mere presence, leading to a unimodal interaction process, resulting in precipitation of the complex. A further remark on this feature will be made in the concluding section. The $\Gamma^{c_1}_{max} < \Gamma^{cmc}_{max}$ and the consequent $A^{c_1}_{min} > A^{cmc}_{min}$ (Table 1) can be ascribed as a consequence of the reduced compactness of the interfacial monolayer at the air/solution interface in the presence of BSA, which arises out of the finite presence of the solubilized BSA−ATAB complex at the interfacial monolayer, as depicted in Scheme 2.

The circular dichroism spectrum of protein in the 200−250 nm range probes the amide transitions at the biopolymer backbone. The α-helix structure is characterized by negative peaks at 208 nm (Figure 2A, solid line). The data were processed using k2d software, which is basically an optimization protocol to create the observed spectrum from a linear combination of three individual spectrum for a known ∼100% α-helical, ∼100% $\beta$-sheeted, and ∼100% random coil protein. The weightage of each individual known spectrum reflects the weightage of the particular structural motif in the studied protein under the solution condition. For pure BSA, 67% helix content was observed, which is consistent with earlier reports. Decrease in helix content on addition of ATAB was observed even before the appearance of turbidity ($c_0$), and very low helix content (∼15%) beyond $c_1$ supports our previous propositions of denaturation of native BSA structure during different stages of the interaction process. The helix content during the different course of BSA−ATAB interaction is given in Table 1. The aromatic region of protein CD spectrum (250−320 nm) probes the environment of the peripheral tryptophan and tyrosine residues. Ellipticity at 256, 292, and 304 nm increases on addition of ATAB (Figure 2B).

The relative viscosity of ATAB in buffer solution (pH 7 and $\mu = 0.015$ M) produced a minimum at 0.16, 0.50, and 5.65 mM CTAB, TTAB, and DTAB, respectively, with varying the respective ATAB concentration in the absence of BSA (Figure 3, crossed squares). The $\eta_{rel}$ values increased thereafter. The initial decrease in $\eta_{rel}$ is mainly augmented by the breakdown of water structure by the quarternary ammonium headgroups of ATABs,[46,51] and thus, $\eta_{rel}$ at $c_{min}$ decreased with higher chain length because of increased perturbation on the water structure. This effect was masked in the presence of BSA (Figure 3, open square), where unfolding of the biopolymer by the action of ATABs contributed to an appreciable increase in viscosity. The denaturation of BSA, from the very beginning of DTAB addition, was discovered by Kelley and McClements using the differential scanning calorimetry (DSC) technique.[37] Breakpoints in the viscometric plots for BSA−ATAB interaction profiles reflected saturation of the biopolymer with ATABs in bulk solution; these were denoted by $c_{sat}$ (Table 1). They were found to closely agree with the microcalorimetric results to be subsequently discussed.

The turbidimetric profiles for the interaction of ATABs with BSA in solution are depicted in Figure 4: the absorbance ($A$) was measured at 450 nm. The $A$ vs log[ATAB] profiles evidenced common features for the studied homologues. The profiles steeply increased from $c_0$ (onset of turbidity) as a result of increased scattering with the advent of coacervation (phase separation), maximized at $c_T$ (maximum turbidity), and then declined to $c_R$ (resolubilization of turbidity, meaning both the completion of solubilization of precipitate and the disappearance of visual turbidity). Onset and disappearance of visual turbidity (coacervation), as marked in the tensiometric profiles, are also marked with crossed and filled square symbols in Figure 4. The results closely resembled one another. In the $A$ vs log[ATAB] profiles, the point $c_T$ corresponded to the onset of dissolution of the

(59) Cabane, B.; Duplessix, R. *Colloids Surf.* **1985**, *13*, 19.
(60) Nagarajan, R. *Colloids Surf.* **1985**, *13*, 1.
(61) Nagarajan, R. *Adv. Colloid Interface Sci.* **1986**, *26*, 205.

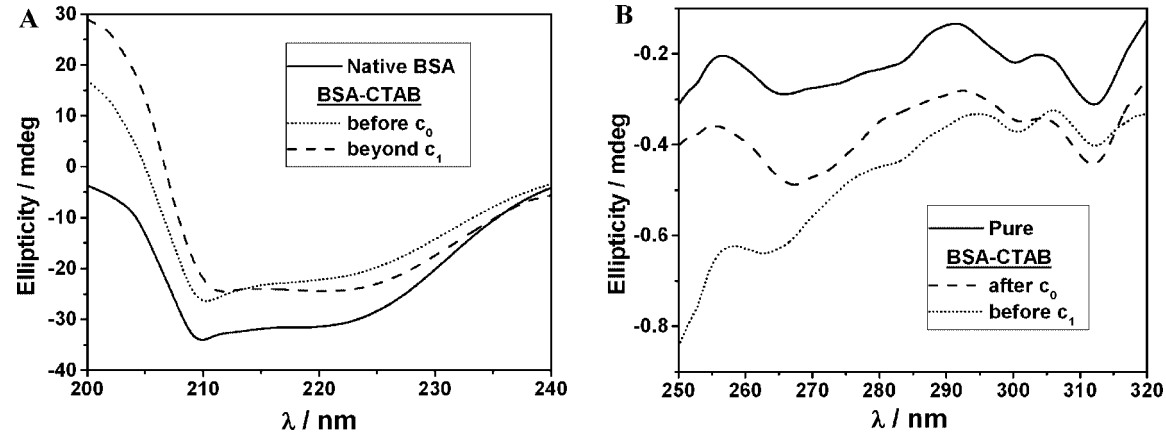


**Figure 2.** Circular dichroic spectrum of BSA at native state and different course (before $c_0$ and after $c_1$) of CTAB addition: (A) far-UV and (B) near-UV region of the spectrum.

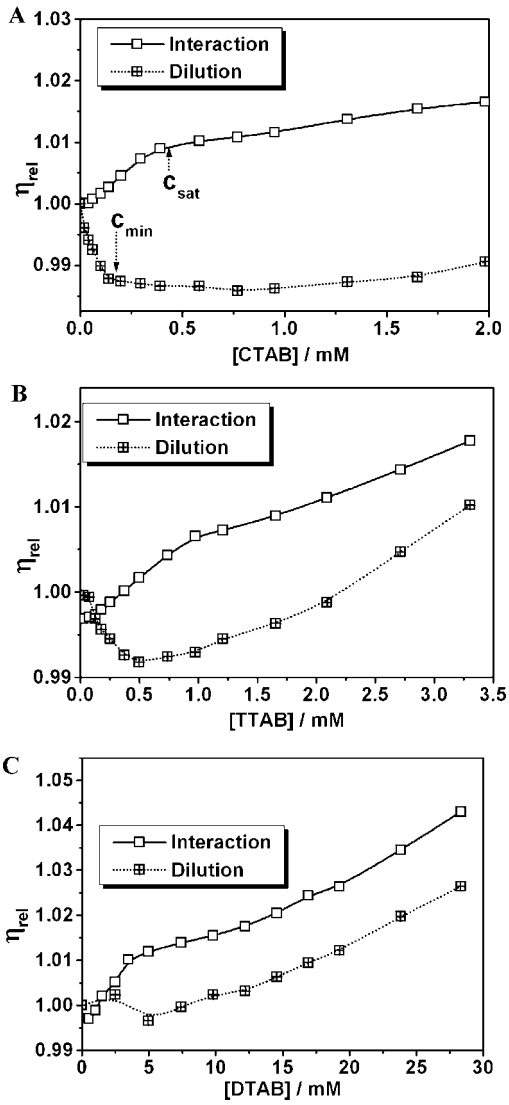


**Figure 3.** Viscometric profiles for 0.025% (w/v) BSA−ATAB interaction in 10 mM phosphate buffer of pH 7 at 303 K: (A) BSA−CTAB, (B) BSA−TTAB, (C) BSA−DTAB. Crossed and open symbols represent ATAB dilution in buffer solution and in BSA solution respectively. $c_{min}$ is also indicated in Figure 2A.

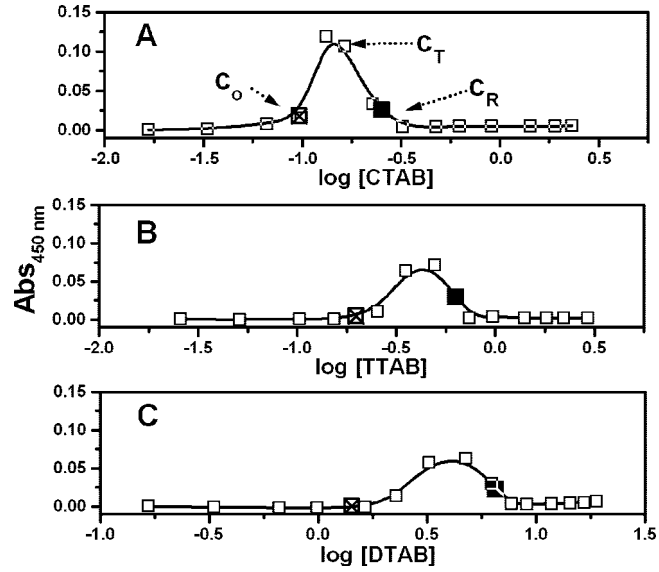


**Figure 4.** Absorbance profiles for 0.025% (w/v) BSA−ATAB interaction in 10 mM phosphate buffer of pH 7 at 303 K. The turbidity appearance point, $c_0$ (crossed symbol); maximum turbidity point, $c_T$; and turbidity disappearance point, $c_R$ (solid symbol), are also indicated in the profile.

coacervate in the micellar hydrocarbon pool,[62] i.e., as the amphiphile aggregates (micelles) are formed in solution, the coacervates can comfortably be accommodated within the hydrophobic core of the aggregated structure (micellar core). The magnitude of $c_T$ followed the order $c_T$DTAB > $c_T$TTAB > $c_T$CTAB (Table 1). At $c_R$, the dissolution of coacervate was complete. Absorbance at $c_T$ ($A_{c_T}$) is a maximum for CTAB and dies down with decreasing chain length (Table 1). This result indicates that higher ATABs are more efficient in binding with BSA under the experimental condition, suggesting the cooperative hydrophobic and electrostatic interaction to lead to the coacervation. Although the log[ATAB] axis is not comparable, the increase in difference between $c_R$ and $c_0$ (Table 1) also reflects that the homologue with higher hydrophobicity is more efficient in more interaction with BSA. The $c_R$ value roughly corroborated with the $c_1$ values by tensiometry, except for DTAB, where $c_1$ was appreciably lower than $c_R$. This concurrence is an outcome of the close proximity between visual resolubilization and $c_1$.

Microcalorimetric studies of BSA−ATAB interaction are again fairly interesting. The discrepancy between the interaction and the dilution profiles lies mainly in the monomeric dilution regime

(62) Nichifor, M.; Lopes, S.; Bastos, M.; Lopes, A. *J. Phys. Chem. B.* **2004**, *108*, 16463.

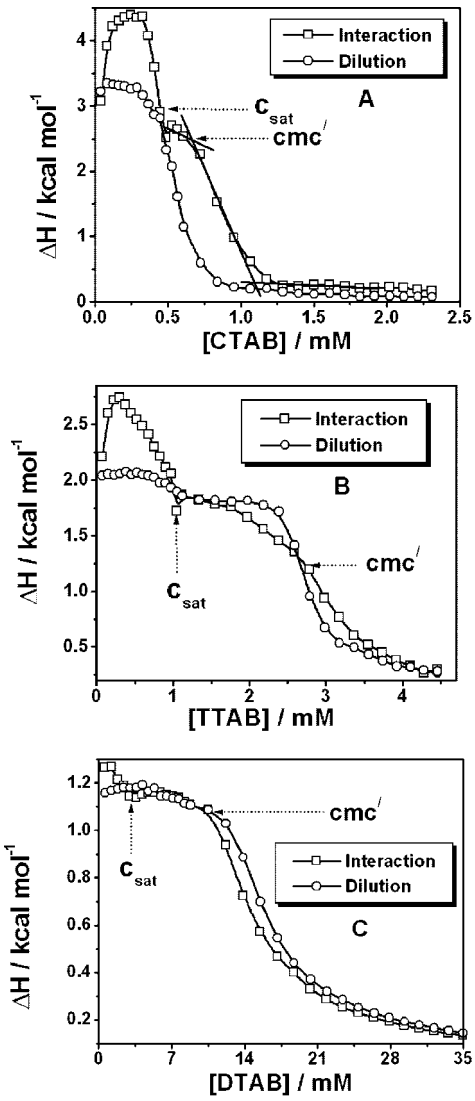


**Figure 5.** Microcalorimetric profiles for 0.025% (w/v) BSA−ATAB (A, CTAB; B, TTAB; and C, DTAB) interaction in 10 mM phosphate buffer of pH 7 at 303 K. Open circle and open square symbols represent ATAB dilution in buffer solution and in BSA solution respectively. $c_{sat}$ and cmc′ are marked in the profile.

of pure surfactant (Figure 5), suggesting that the monomeric adsorption onto the anionic BSA sites is the major contribution, and with aggregated ATAB, BSA hardly interacts. The discrepancy in $\Delta H$ at low ATAB concentration regime is of half the order of enthalpy change associated with the micellar process ($\Delta H_m$), and we expect that the dilution and interaction processes are enthalpically coupled; i.e., interaction enthalpy is not just the difference of observed enthalpy change ($\Delta H_{obs}$) for dilution of concentrated surfactant solution in the presence of BSA and $\Delta H_m$. Individual dilution enthalpograms in buffer and buffered BSA solution are a more realistic interpretation compared to the difference enthalpogram ($\Delta H = \Delta H_{obs} - \Delta H_m$), where the preassumption is that the enthalpic response for the dilution of concentrated micellar solution of surfactant is the same in buffer solution and in the buffered BSA solution taken in the reaction cell; i.e., the presence of the polymer can affect the dilution enthalpogram in the absence of the polymer in no way. Physicochemically, monomeric adsorption being the most pronounced interaction phenomenon even in terms of $\Delta H$ in BSA−ATAB interaction, it is not legitimate to express the process with difference enthalpograms. The [ATAB] corresponding to the onset of pronounced exothermic step is considered as cmc′ in the presence of BSA. It was found from Table 1 that cmc and cmc′ are very close for BSA−TTAB and BSA−DTAB interaction. The exothermic enthalpy change for the micellization process ($\Delta H_m$) decreases only slightly (increases for DTAB) in presence of BSA.

The initial endothermic process corroborates expulsion of water of solvation of BSA by the competitive adsorption of ATAB. For BSA−CTAB interaction, the endothermic hump attains a maxima at 0.23 mM (Figure 5), which is an accidental matching (not observed for TTAB and DTAB) with the $c_1$ value observed tensiometrically (Table 1) and decreases thereafter up to 0.46 mM; we expect that this [CTAB] corresponds to the saturation binding concentration ($c_{sat}$) of ATAB in bulk solution. The added surfactants beyond this concentration are engaged in free micelle formation in CTAB-saturated BSA solution and, therefore, closely follows the dilution enthalpogram. Calorimetrically, cmc′ was taken as the point of intersection between two tangents drawn at the premicellar zone and at the micellization zone, as shown by gray lines in Figure 5A. For BSA−CTAB interaction, cmc′ (0.68 mM) is greater compared to cmc (0.42 mM) for pure CTAB, which can be explained on the basis of the lower concentration of free CTAB in presence of BSA, as expected for coacervation process. For BSA−TTAB interaction, the nature of the interaction profile follows similar nature as the BSA−CTAB system. The initial endothermic peak maximized at 0.29 mM and ends up at 1.05 mM, corresponding to $c_{sat}$. The cmc′ (2.7 mM) value is very close to the cmc value (2.39 mM). For BSA−DTAB interaction, the initial endothermic process was not observed, probably due to higher DTAB:BSA molar ratio at initial stages of the experiment. An exothermic feature ultimately ends up very close to ($c_{sat}$ = 3.44 mM) the dilution profile. The cmc′ (10.43 mM) was observed to be very close to the cmc (11.97 mM).

Coacervation of the BSA−ATAB complex resulted from desorption of water of solvation as a result of monomeric adsorption of $ATA^+$ onto the charged sites on BSA surface. The increased degree of interaction with increasing alkyl chain length indicates that the hydrophobic interaction reinforces the Coulombic attraction. The presence of the initial hump for both CTAB and TTAB reflected a similar type of interaction which is only faintly present in the BSA−DTAB interaction profile. The close resemblance between cmc′ and cmc for TTAB and DTAB, however, reflects only feeble interaction of the lower two homologues with BSA. The enthalpy change corresponding to the initial exothermic peak also decreases in the order CTAB > TTAB > DTAB, as expected from increased hydrophobic interaction. Close resemblance between the interaction and dilution profiles beyond $c_{sat}$ for ATAB also reflected unimodal BSA−ATAB interaction. It is observed that $c_{sat} < c_1$ for CTAB and TTAB, reflecting the interaction process continuing in the bulk solution, even after interfacial saturation, and for DTAB, $c_{sat} < c_1$, which signifies interfacial adsorption prior to completion of the bulk interaction. This is due to the lower hydrophobicity of DTAB and hence of BSA−DTAB complex compared to the higher homologues. Although Bordbar and co-workers reported bimodal BSA−DTAB interaction at pH 7 using ion-selective membrane electrode[63] and calorimetry,[39] we observed a unimodal interaction as also reported by Kelley and McClements[37] using the calorimetric experiments.

**BSA−$C_{12}E_5$ Interaction.** Tensiometric profile for dilution of $C_{12}E_5$ in buffer solution (Figure 6A, crossed symbols) reaches its saturation at $\gamma$ = 30.7 mN $m^{-1}$ (cmc 0.04 mM). The initial

(63) Rafati, A. A.; Bordbar, A.-K.; Gharibi, H.; Amini, M.-K.; Safarpour, M.-A. *Bull. Chem. Soc. Jpn.* **2004**, *77*, 1111.

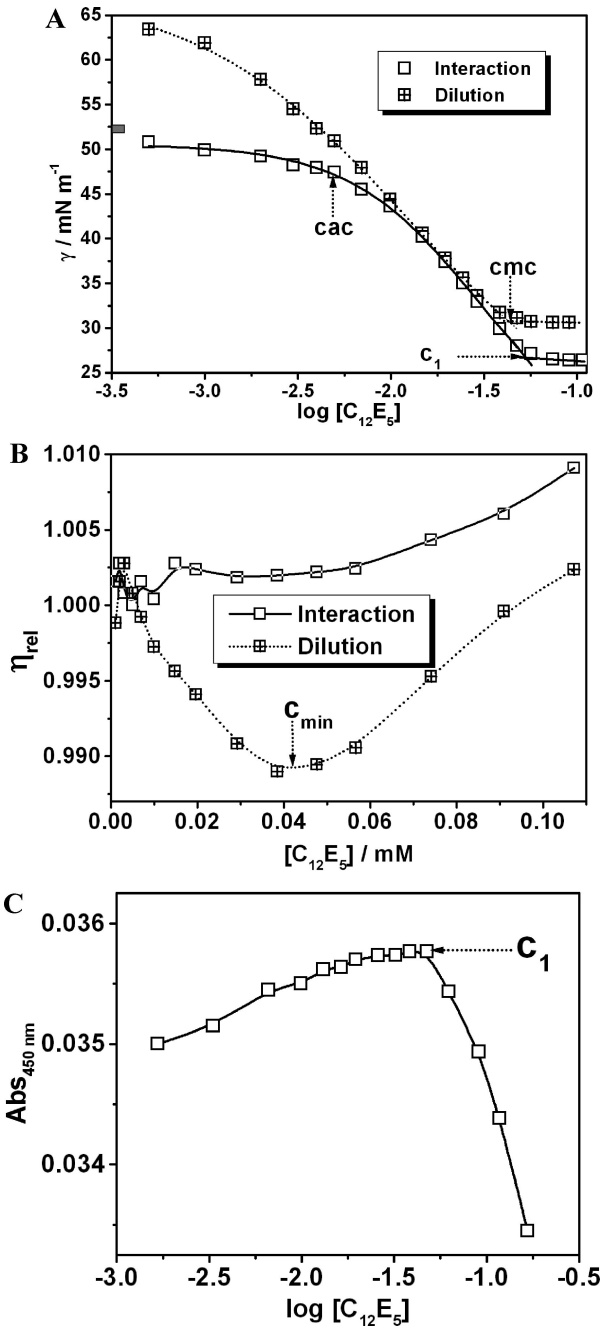


**Figure 6.** 0.025% (w/v) BSA−$C_{12}E_5$ interaction in 10 mM phosphate buffer of pH 7 at 303 K: (A) tensiometry, (B) viscometry, and (C) turbidimetry. Crossed and open symbols represent $C_{12}E_5$ dilution in buffer solution and in BSA solution, respectively. Corresponding break points are indicated in the profiles.

$\gamma$ value for the interaction profile (Figure 6A, open symbols) is lower than that of the dilution profile, reflecting the surface activity of BSA. At the low $C_{12}E_5$ regime (up to cac), the $\gamma$ value of the solution remained more or less unaffected, signifying that $C_{12}E_5$ cannot interact with the interfacially adsorbed BSA at this concentration range. Therefore, cac signifies the onset of interaction at the air/solution interface. Similarity in tensiometric pattern for both the dilution and interaction isotherms in between cac and $c_1$ reflects a weak interaction between the polymer−surfactant pair. Observed interfacial saturation of the interaction profile ($c_1$) occurs at somewhat higher [$C_{12}E_5$] compared to the dilution profile (cmc), reflecting effective interaction and indicating that the distribution constant of the BSA−$C_{12}E_5$ complex ($K_D = ([BSA - C_{12}E_5]_{bulk})/([BSA - C_{12}E_5])_{interface}$) has a large value. The lower interfacial tension ($\gamma_{c_1}$) corresponding to saturation concentration ($c_1$) compared to $\gamma_{cmc}$ reflected the enhanced surface activity of the surfactant in the presence of BSA and also indicates the participation of the biopolymer in interfacial saturation.

Viscometric study of dilution of $C_{12}E_5$ (Figure 6B, crossed symbols) produced a pronounced dip (decreases up to $c_{min} \sim 0.04$ mM and increases thereafter), as observed for ATAB. The depression in $\eta_{rel}$ is absent in the interaction profile (Figure 6B, open symbol) and $\eta_{rel}$ remained more or less constant all throughout. The suppression of the initial depression and constancy thereafter of the interaction profile signifies that $C_{12}E_5$ may be efficient in unfolding the native BSA structure at very low [$C_{12}E_5$].

In turbidimetry measurement, the absorbance at 450 nm moderately increased up to 0.05 mM ($\approx c_1$) and decreased sharply thereafter (Figure 6C). The coacervate started dissolving in the free micelle formed in solution.

Microcalorimetric experiments for dilution of concentrated solution of $C_{12}E_5$ in buffer and BSA solution did not respond because of very low enthalpic response, as observed for most nonionic surfactants.

**BSA−SDS Interaction.** Surface tension of a buffer solution decreases linearly within the studied concentration range with increasing natural logarithm of SDS concentration in solution to reach saturation at cmc (6.19 mM) as shown in Figure 7A (crossed symbols). Interaction of the model anionic surfactant SDS with the abundant, stable protein BSA near its isoelectric point (IEP) is amply reported in the literature using tensiometry, spectrophotometry, circular dichroism, calorimetry, etc. Under our studied conditions, the overall surface charge of BSA and SDS headgroup have similar overall charges. The tensiometric profile evidenced bimodal interaction; it (Figure 7A, open symbol) starts from a lower $\gamma$ value, corresponding to the dilution isotherm (Figure 7A, crossed symbols), as expected from the surface activity of BSA. There is an initial decreasing part up to 0.43 mM SDS ($\gamma_{c_{nc}} \sim 36.2$ mN m$^{-1}$). The tensiometric profile thereafter corresponds to a more or less constant $\gamma$ up to 1.89 mM SDS and decreases thereafter to reach the final plateau at 3.97 mM SDS ($\gamma_{c_1}$ nearly equal to 32 mN m$^{-1}$). The initial decrease in $\gamma$ corresponds to monomeric adsorption of SDS on to the peripheral sites of globular BSA, which thereby gains hydrophobicity and ultimately preferentially adsorbs at the air/solution interface (Scheme 3B), resulting in the steep decrease in $\gamma$ and ends up at 0.43 mM. The monomeric adsorption is driven by the special peripheral topology of the globular protein where the cationic amino acid residues are peripherally distributed in such a fashion that the hydrophobic interaction between the hydrophobic peripheral domains (hydrophobic pockets) of globular amino acids are reinforced by the ionic interaction between the anionic headgroup and the cationic amino acid residues. Similar protein−surfactant interaction on the negative side of the IEP was also reported by Park et al.[64] This issue in context of DNA−protein interaction was approached theoretically by Rouzina et al.[65,66] Chen et al.[67] reported that SDS binds to BSA from both ends, i.e., both hydrophobic interaction between the hydrophobic peripheral domain of the folded biopolymer with the alkyl chain of the surfactant and interaction with an ionic headgroup of the surfactant are operative simultaneously. Kelley and McClements[37] also reported such an monomeric SDS

(64) Park, J. M.; Muhoberac, B. B.; Dubin, P. L.; Xia, J. *Macromolecules* **1992**, *25*, 290.
(65) Rouzina, I.; Bloomfield, V. A. *J. Phys. Chem.* **1996**, *100*, 4292.
(66) Rouzina, I.; Bloomfield, V. A. *J. Phys. Chem.* **1996**, *100*, 4305.
(67) Chen, A.; Wu, D.; Johnson, C. S. *J. Phys. Chem.* **1995**, *99*, 828.

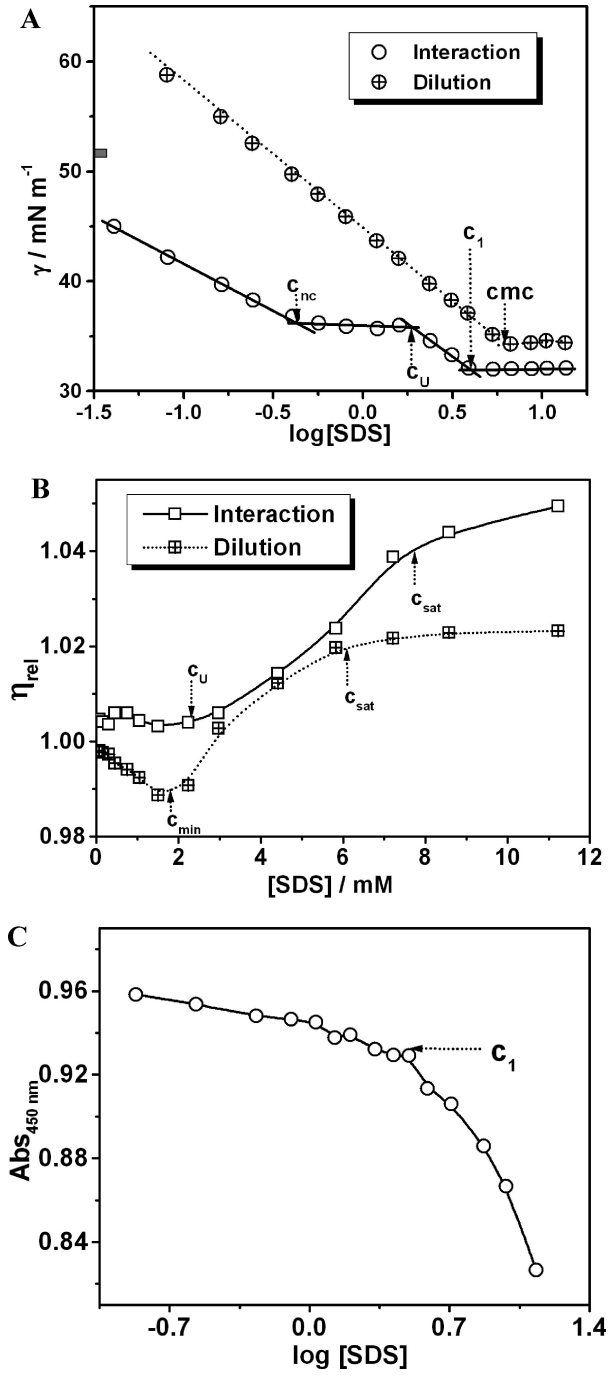


**Figure 7.** 0.025% (w/v) BSA−SDS interaction in 10 mM phosphate buffer of pH 7 at 303 K: (A) tensiometry, (B) viscometry, and (C) turbidimetry. Crossed and open symbols represent SDS dilution in buffer solution and in BSA solution, respectively. Corresponding break points are indicated in the profiles.

adsorption onto the peripheral sites of globular BSA operative at lower [SDS] regime, which is also in line with the circular dichroic report of Takeda et al.[68] The increased thermal stability of native BSA structure in the presence of small SDS concentration is a consequence of the above-mentioned special peripheral topology of BSA native structure. The following plateau corresponds to noncooperative binding[26] (we, therefore, designate the break point at 0.426 mM as $c_{nc}$) of SDS with BSA reflecting the increase in surfactant pressure required for the denaturation

**Scheme 3. BSA−SDS Interaction Is Bimodal**[a]

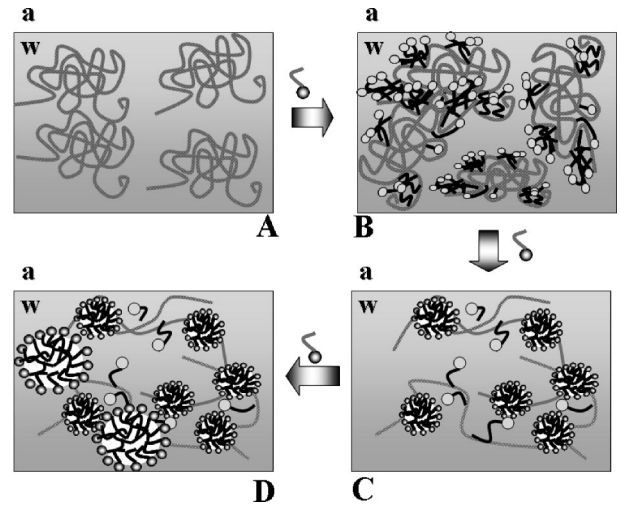


[a] The first step involves monomeric binding with BSA, keeping its native conformation intact. In the second stage, monomeric and aggregated SDS add on to unfold the globular protein structure; finally, free SDS micelles coexist with the BSA−SDS complex.

of the native BSA structure, i.e., instability of the native globular structure of BSA in presence of increased SDS concentration, and continues up to $c_U$ ([SDS] corresponding to unfolding of the peripherally saturated globular BSA). The denaturation process (Scheme 3C) is driven by the fact that surfactant cannot interact with the interior BSA sites due to the very low dielectric constant of the interior phase.[69] The increased number of binding sites provided by this unfolding process invites the coherent second mode of BSA−SDS interaction. During this process, the initially adsorbed monomeric SDS led to an increase in local [SDS] near the vicinity of BSA and induces formation of smaller aggregation[26,28] well below the cmc of pure SDS in absence of the biopolymer under similar solution conditions. The second mode of BSA−SDS interaction, therefore, comprises the adsorption of SDS on BSA sites in both monomeric and lower aggregated forms. The increased hydrophobicity of the polymer−surfactant aggregate induces efficient interfacial adsorption of the polymer−surfactant complex, and the formation of pure surfactant monolayer is restricted, as observed in our previous study[46] of pepsin (IEP ∼ 3)−CTAB interaction at higher pHs. The persistence of BSA−SDS complex at the interfacial monolayer even beyond $c_1$ is evidenced in a lower $\gamma_{c_1}$ value compared to $\gamma_{cmc}$ values as evidenced from Figure 7A and Table 3. The saturation in $\gamma$ during this second mode of interaction reflects the completion of the BSA−SDS interaction. A further increase in SDS concentration led to micellization of the pure surfactant in the bulk solution. As this process cannot perturb the BSA−SDS-saturated interfacial monolayer, it was not perceptible in the tensiometric experiments.

The lower $\Gamma^{c_1}_{max}$ and hence enhanced $A^{c_1}_{min}$ value for dilution of SDS in BSA compared to that in buffer indicated a relaxed monolayer that is probably due to the flexibility of the unfolded BSA. A decrease in $c_1$ compared to cmc under identical solution conditions points to greater hydrophobicity and concomitant enhanced efficacy of the BSA−SDS complex toward interfacial saturation, as also reported previously for protein−surfactant interaction.[46,70,71] In an earlier work, Shweitzer et al.[26] reported

(68) Takeda, K.; Moriyama, Y.; Hachiya, K. In *Interaction of Protein with Ionic Surfactant. Encyclopedia of Surface and Colloid Science*; Marcel Dekker, Inc.: New York, 2002; pp 2558.

(69) Peyere, V.; Lair, V.; Andre, V.; la Marie, G.; Kragh-Hansen, U.; le Maire, M.; Moller, V. *Langmuir* **2005**, *21*, 8865.

(70) Lad, M. D.; Ledger, V. M.; Briggs, B.; Green, R. J.; Frazier, R. A. *Langmuir* **2003**, *19*, 5098.

**Table 2. Critical Micellar Concentration (cmc) and Other Physicochemical Parameters of Pure $C_{12}E_5$ and the Interaction of $C_{12}E_5$ with 0.025% BSA at pH 7 Using Different Techniques at 303 K**

| methods | pure $C_{12}E_5$ | | interaction | |
|---|---|---|---|---|
| surface tension | cmc/mM | 0.043 | cac/mM | 0.008 |
| | $\gamma_{cmc}$/mN m$^{-1}$ | 30.7 | $c_1$/mM | 0.053 |
| | $\Gamma^{cmc}_{max} \times 10^6$/ mol m$^{-2}$ | 1.96 | $\gamma_{cac}$/mN m$^{-1}$ | 46.9 |
| | $A^{cmc}_{min}$/nm$^2$ molecule$^{-1}$ | 8.47 | $\gamma_{c_1}$/mN m$^{-1}$ | 26.4 |
| | | | $\Gamma^{c_1}_{max} \times 10^6$/ mol m$^{-2}$ | 2.12 |
| | | | $A^{c_1}_{min}$/nm$^2$ molecule$^{-1}$ | 7.83 |
| viscometry | $c_{min}$/mM | 0.04 | – | – |
| turbidimetry | – | – | $c_1$/mM | 0.05 |

**Table 3. Critical Micellar Concentration (cmc) and Other Physicochemical Parameters of Pure SDS and the Interaction of SDS with 0.025% BSA at pH 7 Using Different Techniques at 303 K**

| methods | pure SDS | | interaction | |
|---|---|---|---|---|
| surface tension | cmc/mM | 6.19 | $c_{nc}$/mM | 0.43 |
| | $\gamma_{cmc}$/mN m$^{-1}$ | 32.3 | $c_U$/mM | 1.89 |
| | $\Gamma^{cmc}_{max} \times 10^7$/ mol m$^{-2}$ | 21.0 | $c_1$/mM | 3.97 |
| | $A^{cmc}_{min}$/nm$^2$ molecule$^{-1}$ | 7.20 | $\gamma_{c_{nc}}$/mN m$^{-1}$ | 36.2 |
| | | | $\gamma_{c_1}$/mN m$^{-1}$ | 32.0 |
| | | | $\Gamma^{c_{nc}}_{max} \times 10^7$/ mol m$^{-2}$ | 14.8 |
| | | | $\Gamma^{c_1}_{max} \times 10^7$/ mol m$^{-2}$ | 20.4 |
| | | | $A^{c_1}_{min}$/nm$^2$ molecule$^{-1}$ | 8.1 |
| circular dichroism | α-helix content/% | 67 | α-helix content/% | |
| | | | at $c_{nc}$ | 65 |
| | | | at $c_U$ | 53 |
| | | | beyond $c_1$ | 49 |
| viscometry | $c_{min}$/mM | 1.77 | $c_U$/mM | 1.81 |
| | $c_{sat}$/mM | 6.17 | $c_{sat}$/mM | 7.69 |
| turbidimetry | | | $c_1$/mM | 3.60 |
| microcalorimetry | cmc/mM | 4.40 | $c_{nc}$/mM | 0.43 |
| | $\Delta H_m$/ kcal mol$^{-1}$ | −1.0 | $c_U$/mM | 1.89 |
| | | | $c_1$/mM | 3.94 |
| | | | cmc′/mM | 5.55 |
| | | | $\Delta H_{cmc'}$/ kcal mol$^{-1}$ | −1.2 |

an enhancement in $c_1$ (42 mM) of SDS in presence of 0.1% (w/v) BSA (pH 5.4). It was shown that $c_1$was also insensitive to the ionic strength of the solution. This enhanced $c_1$ is probably due to the requirement of more SDS for saturating the biopolymer, as expected from the presence of a larger amount of BSA and an enhanced degree of polymer−surfactant interaction due to the overall zwitterionic form of the biopolymer at IEP.

Relative viscosity ($\eta_{rel}$) for dilution of SDS in buffer solution (Figure 7B, crossed symbols) also initiates by a depression, which thereafter increases gradually and ultimately saturates at ∼6 mM SDS (close to tensiometric cmc in buffer solution), reflecting the micellar dilution process. $\eta_{rel}$ of BSA solution (Figure 7B, open symbols) remained almost unaffected up to ∼2 mM (close to $c_U$, observed tensiometrically) and increases thereafter with increasing [SDS] with a faint break at $c_{sat}$ ∼ 7 mM. The absorption profile (Figure 7C) evidenced a similar feature as BSA−$C_{12}E_5$ interaction,

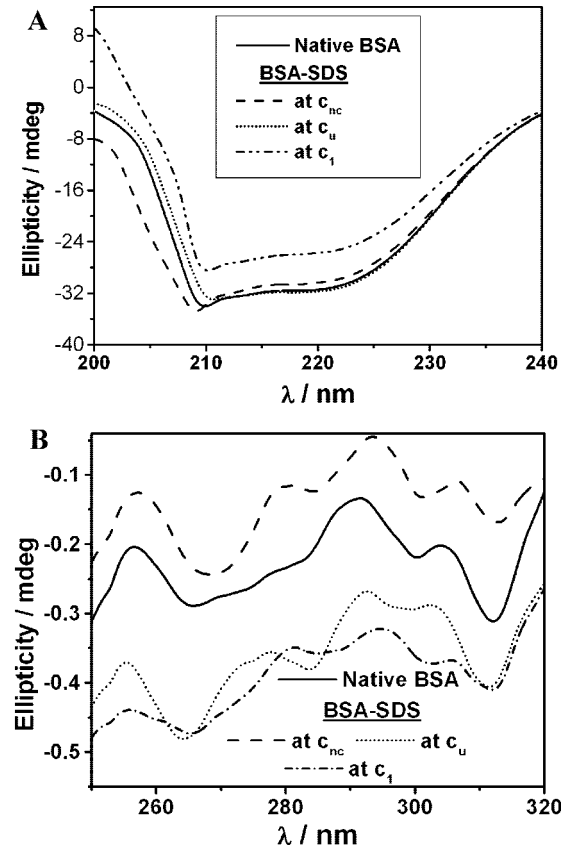


**Figure 8.** (A) Far- and (B) near-UV CD spectrum of BSA at different stages of SDS addition; native BSA, at $c_{nc}$, $c_U$, and $c_{sat}$.

with a break point at 3.6 mM, which is close to $c_1$ observed tensiometrically, and we designate the point with $c_1$.

Circular dichroism spectra in the far-UV region (200−250 nm) indicates (Table 3) retention of native BSA structure upon SDS addition up to $c_{nc}$ (Figure 8A), as reported earlier.[38,72] Beyond $c_{nc}$, the α-helix content of the protein decreases slowly, and at $c_1$, it reaches ∼47%. The near-UV CD spectra (250−320 nm) also indicate greater compactness of the BSA−SDS complex near $c_{nc}$ and a decrease in compactness near $c_U$ and $c_1$ (Figure 8B).

Figure 9 is the microcalorimetric response of dilution of concentrated micellar solution of SDS in buffer (□) and that in buffered BSA (○) solution. Again, the divergence of the two enthalpograms is mainly in the region where SDS is in monomeric form in the reaction cell. The dilution enthalpogram (□) simply consists of the premicellar region with a more or less constant molar enthalpy; in the micellization regime, the molar enthalpy of the overall solution decreases steeply, signifying the change in state of aggregation of the amphiphile aggregates depending on availability of amphiphile, and finally saturates to signify the micellar dilution process. In the interaction profile (○), there is a steep exothermic change over a small but finite range of SDS concentration. The molar enthalpy of the overall solution increases, thereafter forming a shallow crest, and the minimum of it coincides with $c_{nc}$. The endothermic process tends to saturate in terms of molar enthalpy at 1.89 mM, corresponding to $c_U$. The free micellization process starts at 5.55 mM (cmc′), as evident from onset of the sharp exothermic process. The saturation binding, as observed from tensiometry ($c_1$), is not reflected in the individual enthalpograms but is quite evident from the difference enthalpogram as given in inset of Figure 9.

(71) Green, R. J.; Su, T. J.; Joy, H.; Lu, J. R. *Langmuir* **2000**, *16*, 5797.

(72) Jirgensons, B. *Biophys. Acta* **1976**, *434*, 58.

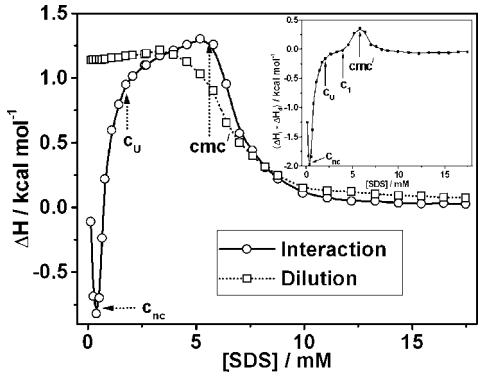


**Figure 9.** Interaction and dilution enthalpograms for 0.025% (w/v) BSA−SDS interaction in 10 mM phosphate buffer of pH 7 at 303 K. The inset shows the difference enthalpograms of BSA−SDS interaction in buffer solution. Corresponding break points are indicated in the profiles.

**Effect of Salinity on BSA−DTAB Interaction.** Addition of NaBr decreases the cmc of ionic surfactant by way of formation of a denser Helmholtz layer, which efficiently screens the electrostatic interaction between the surfactant head groups. On increasing [NaBr], the cmc of DTAB decreases (Figure 10A, inset), whereas Figure 10B shows that the enthalpy of micellization ($\Delta H_m$) remaining fairly unaffected beyond forming a minima in the presence of 10 mM NaBr (Table 4).

Tensiometrically, the cmc of DTAB in buffer solution decreases with increasing [NaBr], as expected. In the presence of BSA, Figure 10A shows that $c_1$ decreases with increasing [NaBr] up to 20 mM and increases at 50 mM NaBr, the $c_1$ values always being lower than the cmc values (Table 4). In the microcalorimetric interaction profiles (Figure 10B), the initial exothermic hump in the enthalpograms diminishes in height with a concomitant decrease in $c_{sat}$, indicating the reluctance of monomeric DTAB binding to BSA sites in the presence of NaBr. The interaction profiles beyond $c_{sat}$ closely resemble the dilution enthalpograms, ensuring only feeble interaction, whereas in presence of 50 mM NaBr, there is a large divergence in dilution profile for SDS between buffer and BSA solution. At this salinity, cmc′ decreases ∼2.5-fold compared to cmc under identical solution conditions. The cmc′ is approximately equal to cmc, even in the presence of 20 mM NaBr. The close resemblance in $\Delta H_m$ and $\Delta H_{cmc'}$ with increasing [NaBr] indicates that the interaction is not enthalpy driven under these circumstances. Electrolytes either inhibit polyanion−surfactant interaction through electrically screening the ionic interaction or enhance the extent of interaction by simultaneously interacting with micelles and the polymer.[73,74] The effect of salt concentration (increasing ionic strength of buffer solution at fixed pH) on BSA−SDS interaction was viscometrically studied by Shinagawa et al.,[33] who reported an increase in intrinsic viscosity of BSA solution on increasing buffer concentration from 10 to 30 mM and a decrease thereafter up to 175 mM. The initial increase was interpreted as a result of increased SDS binding to BSA, as reported earlier by Allen[75] upon increasing [NaCl], and the subsequent decrease was rationalized on the basis of charge neutralization, i.e., an increase in negative charge density onto the biopolymer, which in our case leads to enhanced interaction with the cationic amphiphile. This increased electrostatic potential for interaction increases the affinity of DTAB toward BSA and hence saturates the biopolymer at a lower [DTAB].

## Concluding Remarks

Although BSA−ATAB systems represents oppositely charged polyelectrolyte−surfactant systems, the interaction profile using tensiometry and microcalorimetry are much simpler compared to a BSA−SDS system with similar charges. This is an outcome of the special peripheral topology of BSA in its native state. The cationic amino acid residues are peripherally distributed in such a fashion that the hydrophobic interaction between the alkyl chain of SDS and hydrophobic packets of globular, native BSA is reinforced by the electrostatic attraction between the surfactant headgroup and the cationic amino acids.[37] This topology of native BSA structure increases the stability of native protein structure up to low [SDS]. This topology also increases the thermal stability of the native configuration of BSA against denaturation aided by SDS.[76,77] On the contrary, at neutral pH, the overall −18 surface charge[52] on the protein invites cationic surfactants through Coulombic interaction. The stabilizing effect for BSA−SDS complex is absent for ATABs. Progressive addition of ATABs beyond charge neutralization therefore forces the biopolymer to unfold, resulting in a unimodal interaction, leading to coacervation. The efficiency of ATABs toward unfolding of native BSA structure is also evident from the CD spectroscopy. The coacervates lead to scattering phenomenon and hence a Gaussian plot in $A_{450\ nm}$ vs log[ATAB] profiles. The decrease in the profiles beyond $c_T$ resulted from dissolution of coacervates in micellar core. Among the ATABs, the extent of interaction decreases with decreasing chain length, as expected from the interplay between electrostatic and hydrophobic interactions between the polymer−surfactant pair. The height of the initial hump in the BSA−ATAB interaction enthalpograms also dies down with the decreasing alkyl chain length among the homologues representing the effectiveness of hydrophobic interaction. The close resemblance between the dilution and interaction enthalpograms beyond monomeric adsorption regime indicated feeble interaction of BSA with ATAB in aggregated form. The completion of the initial hump is considered as the saturation concentration for BSA−ATAB interaction. Turbidity of the BSA solution resulted from coacervation, as expected for monomeric adsorption of ATAB on to BSA and consequent desorption of water of solvation. The unaffected tensiometric profile by coacervation process indicates that the process occurs in bulk solution only and hardly hampers the air/solution interface, pointing to unimodal interaction consisting of simultaneous denaturation and interaction of BSA with ATAB in the bulk solution. The decrease in $c_1$ compared to cmc (tensiometry) is another striking feature of this report, which is assumed to be due to the enhanced surface activity of the polymer−surfactant complex after dissolution above IEP, in contrast to earlier reports close to IEP. We observe a decrease in [surfactant], corresponding to saturation in $\gamma$ for all the ionic surfactants, whereas [$C_{12}E_5$], corresponding to interfacial saturation, increases in the presence of BSA, as expected from the widely expected necklace-bead model for polymer−surfactant interaction. Smoothness of the tensiometric interaction isotherm for BSA−$C_{12}E_5$ interaction reflects a unimodal, weak interaction. The increase in $c_1$ compared to cmc of pure $C_{12}E_5$ is a consequence of the greater solubility of the polymer−surfactant complex in the solution. For the BSA−SDS system, the interfacial population of the cationic amino acids results in an initial monomeric interfacial adsorption to the globular biopolymer, and a threshold [SDS] is required to unfold the biopolymer required for the second mode of

(73) Dubin, P. L.; Gruber, J. H.; Xia, J.; Zhang, H. *J. Colloid Interface Sci.* **1992**, *148*, 35.
(74) Xia, J.; Dubin, P. L.; Kim, Y. *J. Phys. Chem.* **1992**, *96*, 6805.
(75) Allen, G. *Biochem, J.* **1974**, *137*, 575.
(76) Magdassi, S.; Vinetsky, Y.; Relkin, P. *Colloids Surf. B.* **1996**, *6*, 353.
(77) Giancola, C.; DeSena, C.; Fessas, D.; Graziano, G.; Barone, G. *Int. J. Biol. Macromolecule* **1997**, *20*, 193.

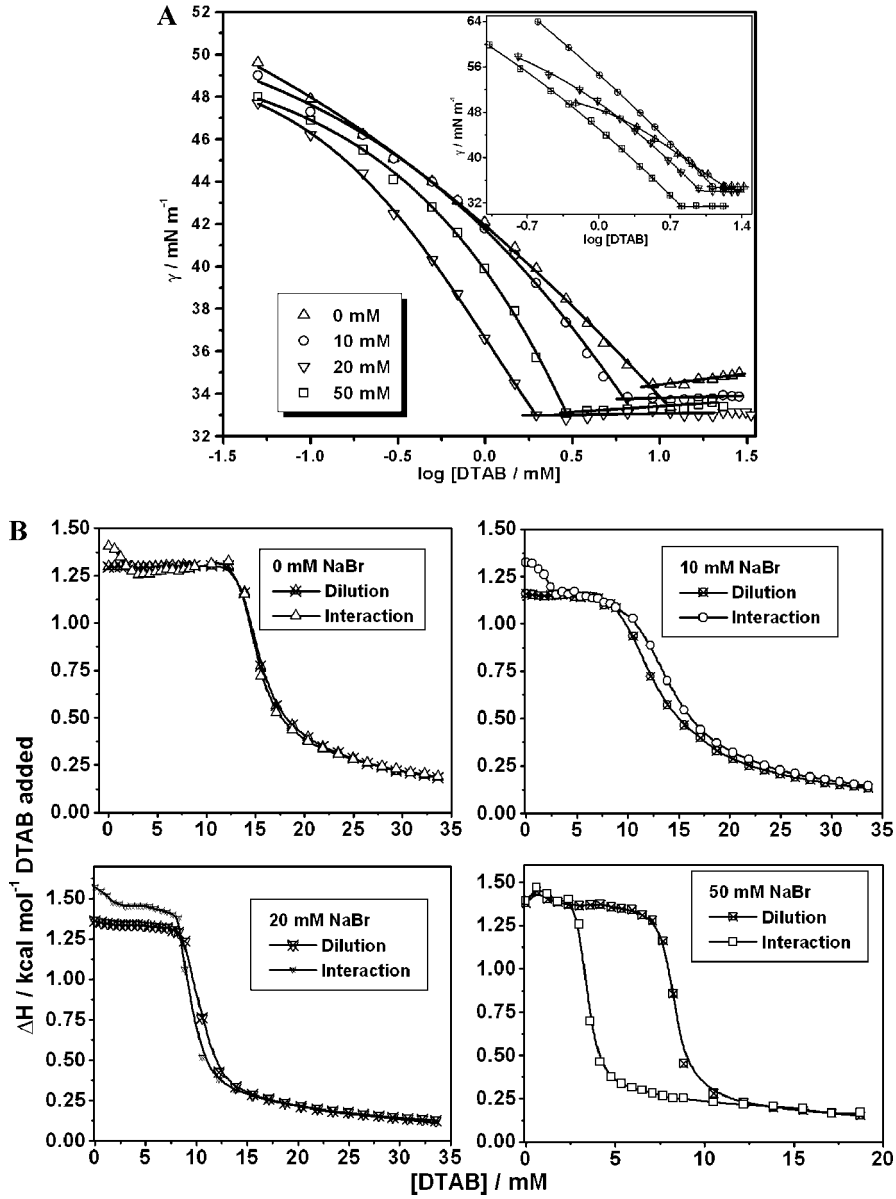


**Figure 10.** (A) Tensiometric (inset shows pure DTAB) and (B) microcalorimetric profiles for 0.025% (w/v) BSA−DTAB interaction in the presence of various amounts of NaBr in phosphate buffer of pH 7 at 303 K.

**Table 4. Critical Micellar Concentration (cmc) and Other Physicochemical Parameters of Pure DTAB and the Interaction of DTAB with 0.025% BSA and Varied [NaBr] at pH 7 Using Different Techniques at 303 K**

| | | parameters | 0 mM NaBr | 10 mM NaBr | 20 mM NaBr | 50 mM NaBr |
|---|---|---|---|---|---|---|
| surface tension | pure | cmc/mM | 16.53 | 13.97 | 9.94 | 6.61 |
| | | $\gamma_{cmc}$/mN m$^{-1}$ | 35.0 | 34.8 | 34.2 | 31.3 |
| | | $\Gamma^{cmc}_{max} \times 10^6$/mol m$^{-2}$ | 1.14 | 1.64 | 1.40 | 1.49 |
| | | $A^{cmc}_{min}$/nm$^2$ molecule$^{-1}$ | 1.46 | 1.01 | 1.18 | 1.11 |
| | interaction | $c_1$/mM | 8.97 | 6.26 | 1.96 | 2.92 |
| | | $\gamma_{c_1}$/mM | 34.4 | 33.8 | 32.9 | 33.2 |
| | | $\Gamma^{c_1}_{max} \times 10^7$/mol m$^{-2}$ | 7.37 | 9.44 | 10.9 | 13.5 |
| | | $A^{c_1}_{min}$/ nm$^2$ molecule$^{-1}$ | 2.25 | 1.76 | 1.52 | 1.23 |
| microcalorimetry | pure | cmc /mM | 12.1 | 11.965 | 8.39 | 7.40 |
| | | $\Delta H_m$/kcal mol$^{-1}$ | −0.9 | −0.7 | −1.0 | −1.1 |
| | interaction | $c_{sat}$/mM | 2.99 | 3.44 | 2.93 | − |
| | | $\Delta H_{c_{sat}}$/kcal mol$^{-1}$ | −0.1 | −0.1 | −0.1 | − |
| | | cmc′/mM | 12.85 | 10.43 | 8.23 | 2.77 |
| | | $\Delta H_{cmc'}$/kcal mol$^{-1}$ | −1.0 | −0.8 | −1.1 | −1.1 |

interaction. The overall process in this case is, therefore, bimodal. Circular dichroic study conclusively evidenced retention of native BSA structure below $c_{nc}$ and partial destruction of α-helix content at $c_U$ and $c_1$. The viscometric study of the BSA−SDS system also supports this information. Interestingly, the concentration-dependent relative viscosity of SDS in buffer saturates at 6.17 mM, and $c_{sat}$ for SDS in the presence of BSA is 7.69 mM. A critical survey of the microcalorimetric enthalpogram evidences

that these concentrations are actually the concentration corresponding to the onset of the micellar dilution process. Therefore, the change in the state of aggregation of SDS micelle under the experimental conditions affects the viscosity of the solution significantly. Therefore, $c_{sat}$ in viscometric BSA−SDS interaction signifies the completion of the change in state of aggregation of the free aggregated SDS structure and not the saturation binding of BSA by SDS. Microcalorimetrically, $c_{nc}$, $c_U$, and cmc′ are obtained clearly, whereas $c_1$ was observable only in the difference plot. The discrepancy between microcalorimetric results between an earlier study[37] is due to the increased molar ratio of the surfactant to biopolymer ratio in the present study. In the previous study, the lower surfactant/BSA range is vividly scanned. In our study, the interaction is studied till the saturation as evident from the approach of both the interaction and dilution enthalpograms, in contrast to the earlier report.[37] The salinity of the medium strongly affects the BSA−DTAB interaction. At lower [NaBr], the interaction decreases, and at higher salinity, the interaction is strengthened.

In all the tensiometric study, $c_1$ represents the saturation (in $\gamma$) concentration. For BSA−ATAB interaction, the concentration of ATAB required for the completion of BSA−ATAB interaction ($c_{sat}$) is greater than $c_1$. This represents not all the BSA−ATAB complexes are able to populate the air/solution interface. However, for $C_{12}E_5$ and SDS, $c_1$ corresponds to saturation in interaction between BSA and the respective amphiphiles. For BSA−$C_{12}E_5$, the complex is more efficient than pure $C_{12}E_5$ in lowering interfacial tension, whereas for BSA−SDS, the interfacial tension of the pure surfactant saturated film is more or less similar to that of the BSA-supported surfactant-saturated film. Moreover, the mode of interaction for the cationic and anionic surfactants are distinctly different. This is due to the peripheral topology of native BSA, where the hydrophobic pockets are adjacent to the cationic amino acid sites, which assists BSA−SDS interaction both electrostatically and hydrophobically. The interaction is bimodal. ATABs, on the other hand, denature BSA at a single step.

**Acknowledgment.** The authors thank Centre for Scientific Research, IACS, Kolkata, for the CD measurements. T.C. thanks CSIR, Government of India, for financial assistance during the tenure of the work, S.P.M. thanks Indian National Science Academy for a Honorary Scientist position. S.G. is a recipient of SERC FAST Track Project (No. SR/FTP/CS-35/2006) from the Department of Science and Technology, Government of India.

LA803797X